Processing and Properties of Advanced Ceramics and Composites VI

Edited by
J. P. Singh
Narottam P. Bansal
Amar S. Bhalla
Morsi M. Mahmoud
Navin Jose Manjooran
Gurpreet Singh
Jacques Lamon
Sung R. Choi
Gary Pickrell
Kathy Lu
Geoff Brennecka
Takashi Goto

Ceramic Transactions
Volume 249

The American Ceramic Society

WILEY

Processing and Properties of Advanced Ceramics and Composites VI

Processing and Properties of Advanced Ceramics and Composites VI

Ceramic Transactions, Volume 249

Edited by
J.P. Singh
Narottam P. Bansal
Amar S. Bhalla
Morsi M. Mahmoud
Navin Jose Manjooran
Gurpreet Singh
Jacques Lamon
Sung R. Choi
Gary Pickrell
Kathy Lu
Geoff Brennecka
Takashi Goto

The American Ceramic Society

WILEY

Copyright © 2014 by The American Ceramic Society. All rights reserved.

Published by John Wiley & Sons, Inc., Hoboken, New Jersey.
Published simultaneously in Canada.

No part of this publication may be reproduced, stored in a retrieval system, or transmitted in any form or by any means, electronic, mechanical, photocopying, recording, scanning, or otherwise, except as permitted under Section 107 or 108 of the 1976 United States Copyright Act, without either the prior written permission of the Publisher, or authorization through payment of the appropriate per-copy fee to the Copyright Clearance Center, Inc., 222 Rosewood Drive, Danvers, MA 01923, (978) 750-8400, fax (978) 750-4470, or on the web at www.copyright.com. Requests to the Publisher for permission should be addressed to the Permissions Department, John Wiley & Sons, Inc., 111 River Street, Hoboken, NJ 07030, (201) 748-6011, fax (201) 748-6008, or online at http://www.wiley.com/go/permission.

Limit of Liability/Disclaimer of Warranty: While the publisher and author have used their best efforts in preparing this book, they make no representations or warranties with respect to the accuracy or completeness of the contents of this book and specifically disclaim any implied warranties of merchantability or fitness for a particular purpose. No warranty may be created or extended by sales representatives or written sales materials. The advice and strategies contained herein may not be suitable for your situation. You should consult with a professional where appropriate. Neither the publisher nor author shall be liable for any loss of profit or any other commercial damages, including but not limited to special, incidental, consequential, or other damages.

For general information on our other products and services or for technical support, please contact our Customer Care Department within the United States at (800) 762-2974, outside the United States at (317) 572-3993 or fax (317) 572-4002.

Wiley also publishes its books in a variety of electronic formats. Some content that appears in print may not be available in electronic formats. For more information about Wiley products, visit our web site at www.wiley.com.

Library of Congress Cataloging-in-Publication Data is available.

ISBN: 978-1-118-99549-5
ISSN: 1042-1122

Printed in the United States of America.

10 9 8 7 6 5 4 3 2 1

Contents

CERAMIC MATRIX COMPOSITES

INNOVATIVE PROCESSING

CONTROLLED SYNTHESIS, PROCESSING, AND APPLICATIONS OF STRUCTURAL AND FUNCTIONAL NANOMATERIALS

ELECTRONIC AND FUNCTIONAL CERAMICS

MATERIALS FOR HARSH ENVIRONMENTS

PROCESSING AND PERFORMANCE OF MATERIALS USING MICROWAVES, ELECTRIC AND MAGNETIC FIELDS

Preface

This volume contains papers presented at seven international symposia held during the Materials Science & Technology 2013 Conference (MS&T'13), October 27-31, 2013 at the Palais des congress, in Montréal, Quebec, Canada. The symposia in this volume include: Innovative Processing and Synthesis of Ceramics, Glasses and Composites; Advances in Ceramic Matrix Composites; Advanced Materials for Harsh Environments; Advances in Dielectric Materials and Electronic Devices; Controlled Synthesis, Processing, and Applications of Structural and Functional Nanomaterials; Rustum Roy Memorial Symposium on Processing and Performance of Materials Using Microwaves, Electric, and Magnetic Fields; and Solution-Based Processing for Ceramic Materials.

These conference symposia provided a forum for scientists, engineers, and technologists to discuss and exchange state-of-the-art ideas, information, and technology on advanced methods and approaches for processing, synthesis, characterization, and applications of ceramics, glasses, and composites.

Thirty-six papers that were discussed at these symposia are included in this proceeding volume. Each manuscript was peer-reviewed using The American Ceramic Society's review process.

The editors wish to extend their gratitude and appreciation to all the authors for their submissions and revisions of manuscripts, to all the participants and session chairs for their time and effort, and to all the reviewers for their valuable comments and suggestions.

We hope that this volume will serve as a useful reference for the professionals working in the field of synthesis and processing of ceramics and composites as well as their properties.

J.P. SINGH
NAROTTAM P. BANSAL
AMAR S. BHALLA
MORSI M. MAHMOUD
NAVIN JOSE MANJOORAN
GURPREET SINGH

JACQUES LAMON
SUNG R. CHOI
GARY PICKRELL
KATHY LU
GEOFF BRENNECKA
TAKASHI GOTO

Ceramic Matrix Composites

FABRICATION OF NOVEL $ZrO_2(Y_2O_3)$-Al_2O_3 CERAMICS HAVING HIGH STRENGTH AND TOUGHNESS BY PULSED ELECTRIC-CURRENT PRESSURE SINTERING (PECPS) OF SOL-GEL DERIVED SOLID SOLUTION POWDERS

Ken Hirota[*1], Kengo Shibaya[1], Masaki Kato[*1], and Hideki Taguchi[2]
[*1] Faculty of Science and Engineering, Doshisha University, Kyo-Tanabe Kyoto 610-0321, Japan
[2] The Graduate School of Natural Science and Technology (Science), Okayama University, Okayama 700-8530, Japan

Keywords: Zirconium oxide; Aluminum oxide; Yttrium oxide; Pulsed electric-current pressure sintering (PECPS); Mechanical properties

ABSTRACT

ZrO_2 based ceramics containing 25 mol% Al_2O_3 and 0.90~1.125 mol% Y_2O_3, *i.e.*, ZrO_2(1.2~1.5 mol%Y_2O_3)-25mol%Al_2O_3 have been fabricated at 1523 to 1623 K (1250~1350°C) for 10 min under 60 MPa in Ar by pulsed electric-current pressure sintering (PECPS) of sol-gel derived cubic ZrO_2 solid solution (*ss*) powders. Dense tetragonal-ZrO_2 (*t*-ZrO_2) phase composite ceramics (≥99.5%) sintered at 1623 K (1350°C), being composed of $\leq \sim\Phi 200$ nm grains, revealed high bending strength $\sigma_b \geq 1.5$ GPa and high fracture toughness $K_{IC} \geq 15.5$ MPa·m$^{1/2}$ simultaneously. Precise investigation has been performed on the relationship between their microstructures and mechanical properties, the former of which depend on the content of Y_2O_3 and calcining temperatures. SEM/TEM observations cleared that these improved mechanical properties might be originated from homogeneous distribution of α-Al_2O_3 particles around the dense *t*-ZrO_2 grain matrix; the precipitation of α-Al_2O_3 could be achieved by adopting the (*ss*) powders and PECPS. The Y_2O_3 content in fine ZrO_2 grains has much effect of controlling the stress-induced transformation toughening of tetragonal to monoclinic ZrO_2.

INTRODUCTION

Since the discovery of ZrO_2-toughening mechanism based on the stress-induced transformation from tetragonal to monoclinic phases by Garvi [1], partially stabilized zirconia (PSZ) with a small amount of Y_2O_3 addition has been much focused, and many studies have been performed on the fabrication of other stabilizer added dense PSZ. In addition to these, $ZrO_2(Y_2O_3)$ based and $ZrO_2(Y_2O_3)/Al_2O_3$ composite ceramics fabricated using hot pressing (HP) and hot isostatic pressing (HIP) have been developed [2-6]. On the other hand, the solid solution (*ss*) in the ZrO_2-Al_2O_3 system has not been paid attention; because it was believed that the ZrO_2-Al_2O_3 system did not form the *ss* even at higher temperatures. However, since the report by Alper [7] on the formation of ZrO_2(*ss*) containing 7mol% Al_2O_3, the sol-gel derived ZrO_2(*ss*) powders were prepared and then 75mol%ZrO_2-25mol%Al_2O_3(*ss*) powders were HIP sintered at 1373 K (1100°C) under 196 MPa for 1 h [8]. Their mechanical properties were evaluated; fracture toughness K_{IC} of 23 MPa·m$^{1/2}$ was achieved, however, their three-point bending strength σ_b was remained as low as 570 MPa. After that, there has been no report on the fabrication of dense monolithic or composite ceramics that show high $\sigma_b \geq 1$ GPa and high $K_{IC} \geq 20$ MPa·m$^{1/2}$ at the same time. If bulk ceramics having both high σ_b and high K_{IC} simultaneously are developed, they can cast aside the concept of "Ceramics are brittle" and spread their application fields widely.

In the present study, we have prepared $ZrO_2(Y_2O_3)$-Al_2O_3(*ss*) nanometer-sized powders by the sol-gel method and densified them with a pulsed electric-current pressure sintering (PECPS) [9], which method is suitable for the fabrication of high-strength dense ceramics consisting of small grain matrix. In addition, to achieve high fracture toughness, we took into account of the transformation toughening of ZrO_2. Based on these concepts, we have considered as follows; 1) the sintering method has been changed from the conventional electric furnace, HP and HIP to PECPS with an extreme high heating rate under strong electric pulse field, which means PECPS would make it possible to fabricate dense ceramics composed of fine grains; 2) we have already achieved high K_{IC} ceramics in the ZrO_2-Al_2O_3 systems [8]; 3) in the $ZrO_2(Y_2O_3)$-Al_2O_3(*ss*) powders, Al_2O_3 also would act as partially stabilizer in the ZrO_2 based ceramics; and 4) it has been reported that 25mo% Al_2O_3 addition improves the bending strength of $ZrO_2(Y_2O_3)$ ceramics [10,11]. Then, we have selected the composition of ZrO_2 (1.2~1.5mol%Y_2O_3)-25mol% Al_2O_3 from the conventional ZrO_2(2.0 ~3.0mol%Y_2O_3) which has been used as the high-toughness ceramics.

EXPERIMENTAL PROCEDURE

Preparation of $ZrO_2(Y_2O_3)$- 25mol%Al_2O_3 ceramics

The preparation of $ZrO_2(Y_2O_3)$-25mol%Al_2O_3 solid solution (*ss*) powders and the fabrication of dense ceramics using these powders are described in previous our paper [8]. The (*ss*) powders with the composition of 75mol%ZrO_2(1.2~1.5mol%Y_2O_3)–25mol%Al_2O_3 [ZrO_2:Y_2O_3:Al_2O_3=74.10~73.875:0.9~1.125:25.0 mol%] were prepared using $Zr(OC_3H_7)_4$ (>99.9% pure), $Y(OC_3H_7)_3$ (>99.9% pure), and $Al(OC_3H_7)_3$ (>99.9% pure), as starting materials [8,12]. The as-prepared powder (precursor) was calcined at 1093K (820°C) for 75mol%ZrO_2(1.5mol%Y_2O_3)-25mol%Al_2O_3 (henceforth, abbreviate as ZrO_2(1.5Y)-25 mol% Al_2O_3 and denote as [1.5Y]) and 1138 K (865°C), 1153 K (880°C) and 1168 K (895°C) for ZrO_2(1.2Y)-25mol%Al_2O_3 ([1.2Y]) composition powders for 1 h in air. As will be described latter, these temperatures were determined based on the crystallization temperatures about 1088 K(815°C) and 1133 K(860°C) for 1.5Y and 1.2Y powders, respectively, from the results of XRD and DTA/TG analyses.

Calcined powder compacts after CIPing at 245 MPa for 3 min were sintered with a pulsed electric-current pressure sintering (PECPS: *SPS-5104A*, SPS SYNTEX INC., Tokyo, Japan) (on-off interval=12:2) with a heating rate of 100 K·min^{-1} (1.667 K/s), at 1523 to 1623 K (1250~1350°C) under 60 MPa in Ar using a carbon mold (ϕ40-ϕ16 -30^h mm) and plunger (ϕ39.9-40^h mm).

EVALUATION OF SAMPLES

Microstructures

Thermal analysis of precursors was conducted using a differential thermal analysis and thermal gravimetry (DT-TG 60H, Shimadzu, Kyoto, Japan) in air with a heating rate of 10 K·min^{-1} (0.1667 K·s^{-1}). Crystalline phases were identified by X-ray diffraction (XRD) analysis (Cu$K\alpha$ radiation, *Rint 2000*, Rigaku, Osaka, Japan). The volume fraction of the monoclinic ZrO_2 (*m*- ZrO_2) phase for the test samples was determined from the intensity ratio of the monoclinic (111) and (11-1) diffraction lines to the tetragonal (111) line by XRD analysis [13]. Bulk densities (D_{obs}) of sintered ceramics after polishing with a diamond paste (nominal size ϕ1~3 μm) were evaluated by Archimedes method. Theoretical densities (D_x) of ceramics were calculated as follows; the lattice parameters of *t*-ZrO_2 phase were estimated to be a=0.360520~0.360657 and c=0.518758~0.518948 nm, and those of *m*-ZrO_2 phase also were a=0.519003~0.518014, b=0.514807~0.5169561, c=0.535040~0.535023 nm, and □=98.6960~98.8594° using Rietveld analysis [14]. Then the values of D_x(*t*-ZrO_2(1.5Y))=6.0510 and D_x(*m*-ZrO_2(1.5Y))=5.7725 Mg·m^{-3} were obtained. From the *t*/*m*-ZrO_2 volume ratios and the values of $D_x(\alpha\text{-}Al_2O_3)=3.987$ Mg·m^{-3} (JCPDS: #10-0173), the D_x values of composite ceramics were calculated. Both $D_x(t\text{-}ZrO_2(1.2Y))$ and $D_x(m\text{-}ZrO_2(1.2Y))$ were assumed to be the same as $D_x(t\text{-}ZrO_2(1.5Y))$ and $D_x(m\text{-}ZrO_2(1.5Y))$, respectively, because of a small difference in Y_2O_3 addition.

Microstructural observation on the as-prepared and calcined powders, and the fractured or polished surfaces of ceramics were conducted using a field emission-type transmission electron microscope (FE-TEM, *JEM-2100F*, JEOL Ltd., Tokyo, Japan) and a scanning electron microscope (FE-SEM, *JSM-7001FD*, JEOL Ltd.) equipped with an energy dispersive spectroscopy (EDS, *JED-2300/T* and *JED-2300/F*, JEOL Ltd., respectively). Before TEM observation, the specimens were processed into thinner using a focused ion beam (FIB, *FB-2200*, Hitachi High-Tech Fielding Co. Ltd., Tokyo, Japan). The grain sizes were determined by an intercept method [15].

Mechanical properties

After crystalline phase identification, test bars (~3×3.5×11 mm^3) for mechanical-property measurements were cut from the ceramics with a diamond cutting-blade and then their four sides were polished to mirror surface with a diamond paste (nominal particle size ϕ1-3 μm). Three-point bending strength (σ_b) was evaluated with a cross-head speed of 0.5 mm·min^{-1} and an 8 mm-span length using WC jigs. Vickers hardness (H_v) and fracture toughness (K_{IC}) were evaluated using a Vickers hardness tester (*HMV*, Shimadzu) with an applying load of 19.6 N and a duration time of 15 s for the former, and the indentation fracture method (IF) with Niihara's equation using a Vickers hardness tester (*VMT-7*, Matsuzawa, Osaka, Japan) with applying load of 196 N and a duration time of 15 s for the latter [16,17].

RESULTS AND DISCUSSION

Characterization of powders and ceramics

Fig. 1 (a) shows a TEM photograph of as-prepared 1.2Y powder; thin fine hallow powders with a particle size of around 0.6 nm was observed.

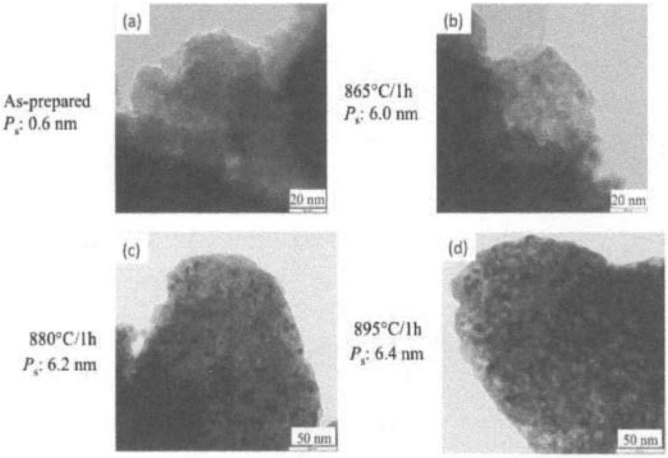

Figure 1. TEM photographs of $ZrO_2(1.2Y)$-25mol%Al_2O_3 powders; (a) as-prepared and calcined for 1 h in air at (b) 865, (c) 880, and (d) 895°C.

DTA-TG curves of this powder were measured (Fig.2); a strong endothermic peak around 1133 K (860°C) was detected. The same as-prepared 1.2Y powder was analyzed using XRD (Fig. 3 (i)); amorphous pattern was observed. And after calcined at 1138 K (865°C) for 1 h, the sample revealed crystallized cubic ZrO_2 phase (Fig. 3(ii)); no other crystalline compounds, such as α-Al_2O_3 and tetragonal- (*t*-) or monoclinic- (*m*-) ZrO_2 phases, were found; informing that cubic (*c*-) ZrO_2 solid solution (*ss*) was crystallized (formed) from the amorphous powder. From this result, it is clear that amorphous solid solution powder transformed into *c*-ZrO_2(*ss*) at crystallization temperature T_x of 1133 K (860°C). Furthermore, 1.2Y powder was calcined at 1153 K (880°C) and 1168 K (895°C) for 1 h to investigate the relationship between the calcined temperatures and the microstructures/mechanical properties of sintered ceramics.

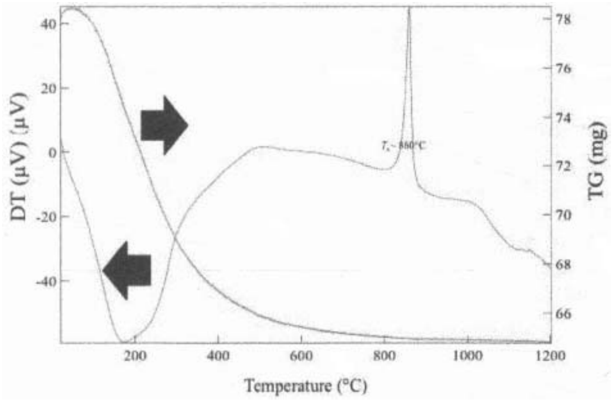

Figure 2. DTA-TG curves of as-prepared ZrO_2 (1.2Y) -25mol%Al_2O_3 (*ss*) powder.

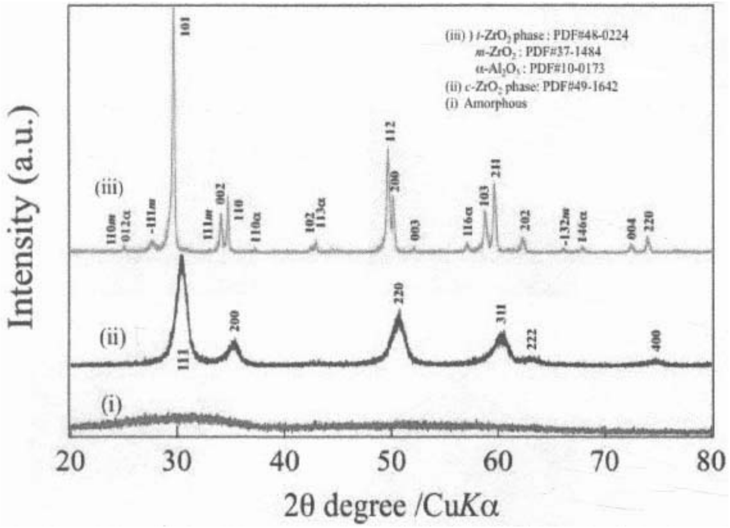

Figure 3. XRD patterns for ZrO_2(1.2Y)-25 mol% Al_2O_3 (*ss*) samples: (i) as-prepared, (ii) calcined at 865°C for 1 h in air and (iii) sintered at 1300°C by PECPS.

Fig. 1 (b)-(d) show the TEM photographs of calcined powders; the particle shape becomes clear and the particle size Ps increased from 0.6 (amorphous) to 6.0 (865°C), 6.2 (880°C) and 6.4 nm (895°C) monotonously. As the same manner, 1.5Y powder crystallized from amorphous (*ss*) to *c*-ZrO_2(*ss*) at T_x of 1093 K (820°C).

Microstructures and mechanical properties of ceramics

Calcined powder compacts were densified using a PECPS as already described. Fig. 3(iii) shows representative XRD pattern of the polished surface of 1.2Y ceramics sintered at 1300°C from 865°C-calcined powder; a main phase changed from *c*-ZrO_2(*ss*) to *t*-ZrO_2, *m*ZrO_2 and α-Al_2O_3. Diffraction peaks are indexed based on each PDF file (*t*-ZrO_2:#48-0024, *m*ZrO_2:#37-1481, α-Al_2O_3:#10-0173). From these XRD line intensity data, *t*-ZrO_2 vol% was calculated using Garvie & Nicholson's equation [13]; in the present study, main phase of other ceramics is also *t*-ZrO_2, as will be shown in the latter.

Fig. 4 displays the representative microstructural parameters, such as (a) *t*-ZrO_2 phase volume ratio *t*-ZrO_2 (vol%), (b) average grain sizes G_s, (c) bulk density D_{obs}, and relative density of D_{obs}/D_x of the 1.2Y ceramics using 865°C calcined powder. Little change in *t*-ZrO_2 (vol%) is observed and stable around 96.5vol% as shown in XRD pattern on 1300°C sintered ceramics (Fi. 3 (iii)), however, the G_s increased rapidly with increasing sintering temperature more than 1325°C. On the other hand, D_{obs} and D_{obs}/D_x revealed the maximum values at 1300°C; the value of D_{obs}/D_x reached ≥ 99.5%. The mechanical properties of 1.2Y ceramics sintered at 1300 and 1350°C are shown as a function of calcining temperatures (Fig. 5).

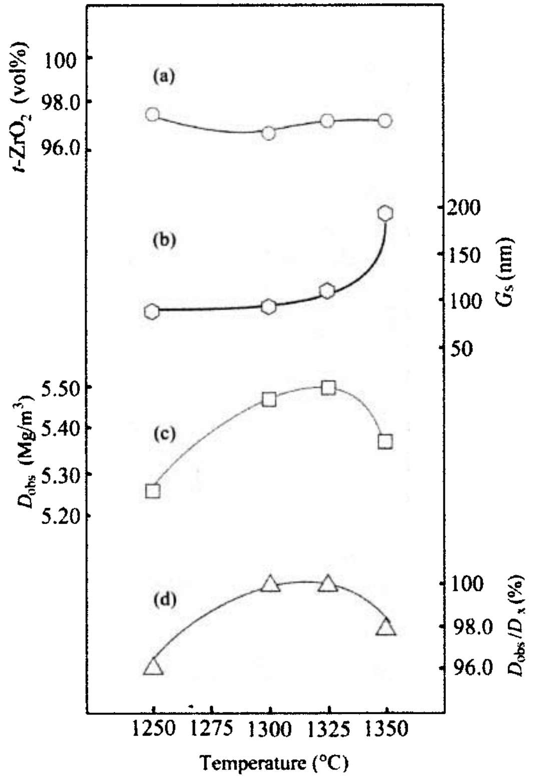

Figure 4. Microstructural properties of ZrO_2(1.2Y)- 25 mol%Al_2O_3 composites fabricated from 865°C calcined powders.

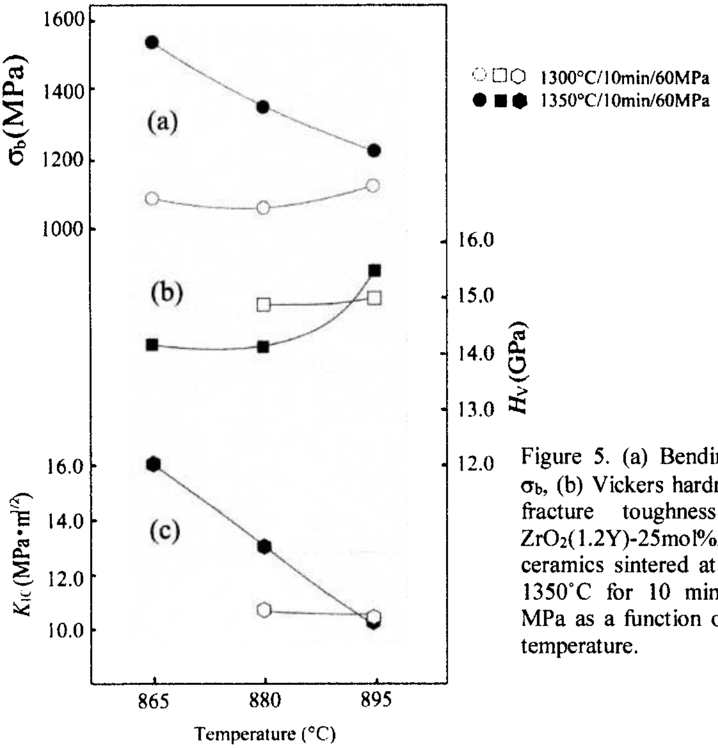

Figure 5. (a) Bending strength σ_b, (b) Vickers hardness H_v, (c) fracture toughness K_{IC} of ZrO_2(1.2Y)-25mol%Al_2O_3 ceramics sintered at 1300°C or 1350°C for 10 min under 60 MPa as a function of calcining temperature.

Bending strength σ_b of ceramics in Fig. 5(a) reveals two distinctive characteristics; i) higher (1350°C) sintering temperature gave high values, ii) there is much calcining temperature dependence of σ_b, especially, in the high-temperature sintered (1350°C) ceramics. It should be noted that the best σ_b value reached ~15.5 GPa with the ZrO_2(1.2Y)-25mol%Al_2O_3 ceramics. On the contrary, Vickers hardness H_v (in Fig. 5 (b)) demonstrates an inverse tendency on sintering temperature: low-temperature (1300°C) sintered ceramics reveal higher H_v value of ~14.8 GPa, this might be originated from the small grain sizes induced by low temperature sintering. In Fig. 5 (c), very important property for engineering ceramics, fracture toughness K_{IC}, is displayed as a function of calcining temperature. At a glance, almost nearly the same tendency as shown in σ_b is observed; i) higher the sintering temperature, higher K_{IC} values. And ii) lower- calcining temperature resulted in higher K_{IC}, which reached ~16.0 MPa·m$^{1/2}$.

Here, up to now it has been believed that both high strength and high toughness of ceramics could not be performed, as if there is a "trade-off relation" between them. However, both high σ_b ($\geq$15.5 GPa) and K_{IC} ($\geq$16.0 MPa·m$^{1/2}$) have been achieved in the same ceramics simultaneously for the first time.

To investigate the calcination temperature dependence of mechanical properties above mentioned, their microstructures, especially focused on the distribution and size of α-Al_2O_3 grains because we thought that strength and toughness have been much affected by the guest grains in the composite ceramics. Fig. 6 (a)-(c) display the SEM photographs of polished surfaces of 1.2Y ceramics fabricated from various calcining powders, indicating dense and homogeneous microstructures irrespective calcining temperature. However, in Fig. 6 (d)-(f), there is some difference among them, higher the calcination temperature, smaller the grain size and homogenous the α-Al_2O_3 black grains. In general, the dense ceramics composed of fine grains can reveal higher strength. These photographs proved the dependence of calcining temperature on the mechanical properties in Fig. 5(a).

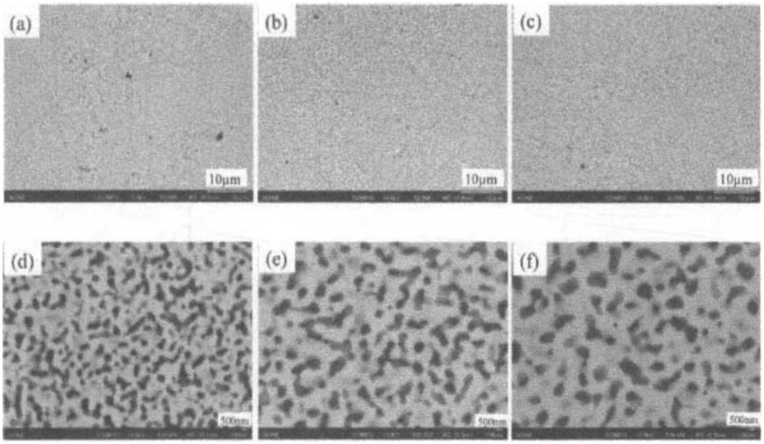

Figure 6. SEM photographs of the polished flat surfaces of ZrO_2(1.2Y)-25mol%Al_2O_3 ceramics sintered at 1350°C using the powders calcined at (a,d) 865°, (b,e) 880°, and (c,f) 895°C for 1 h in air. (a)~(c): low and (d)~(f) high magnifications.

In Fig. 7, the mechanical properties (σ_b, H_v, K_{IC}) of two kinds of ceramics, 1.5Y and 1.2Y, are displayed as a function of sintering temperature. First of all, it is recognized easily that 1.5Y ceramics show higher values, except for H_v, in all sintering temperature. 1.5Y ceramics demonstrate extreme high strength σ_b up to ~1.6 GPa at the same time high K_{IC} value of ~18.4 MPa·m/$^{1/2}$. Furthermore, when we focus on the K_{IC} value, 1.5Y ceramics reveal marvelous value more than 20 MPa·m$^{1/2}$, *i.e.*, ~21.3 MPa·m/$^{1/2}$, in addition, their σ_b value reaches ~13.3 GPa. A little bit "trade-off relation" is observed in the 1.5Y ceramics. Thus, note that dense tetragonal-ZrO_2 (*t*-ZrO_2) phase composite ceramics (≥99.5%) sintered at 1623 K (1350°C), being composed of ≤ ~Φ200 nm grains, revealed high bending strength σ_b ≥1.5 GPa and high fracture toughness K_{IC} ≥15.5 MPa·m$^{1/2}$ simultaneously.

FE-SEM microstructural observation on the fracture surfaces of 1.2Y-1300°C (Fig. 8(a)), 1.2Y-1350°C (Fig. 8(b)), 1.5Y-1300°C (Fig. 8(c)), and 1.5Y-1350°C (Fig. 8(d)) has been performed; these ceramics have been fabricated from 865°C-calcined 1.2Y and 820°C-calcined 1.5Y powders, respectively. These ceramics show dense texture and are consisted of fine grains (100-200 nm); here, we easily take notice of the grain size difference between 1.2Y-1350°C and 1.5Y-1350°C ceramics. This microstructural difference also support that the higher strength could be achieve in 1.5Y-1350°C ceramics due to the smaller grain size. FE-TEM equipped with EDS analysis was used to investigate the microstructures precisely from the viewpoint of grain's chemical composition. Fig. 9 (a) and (b) show the microstructure of 1.5Y ceramics sintered at 1300°C and elemental EDS-line analysis data on the same position, respectively; from (a) it is clear that dense microstructure consisting of large/small black and white grains was observed. Black and white grains correspond to ZrO_2 and Al_2O_3, respectively, which is in inverse to the SEM photographs. In Fig. 9 (b) of the EDS analysis along the upper line elemental spectra of Zr, Y, O, and Al are shown from the upper to the bottom. From these analytical results, it was cleared that black or grey grains contained Zr, Y, and O, and whittle grains Al and O.

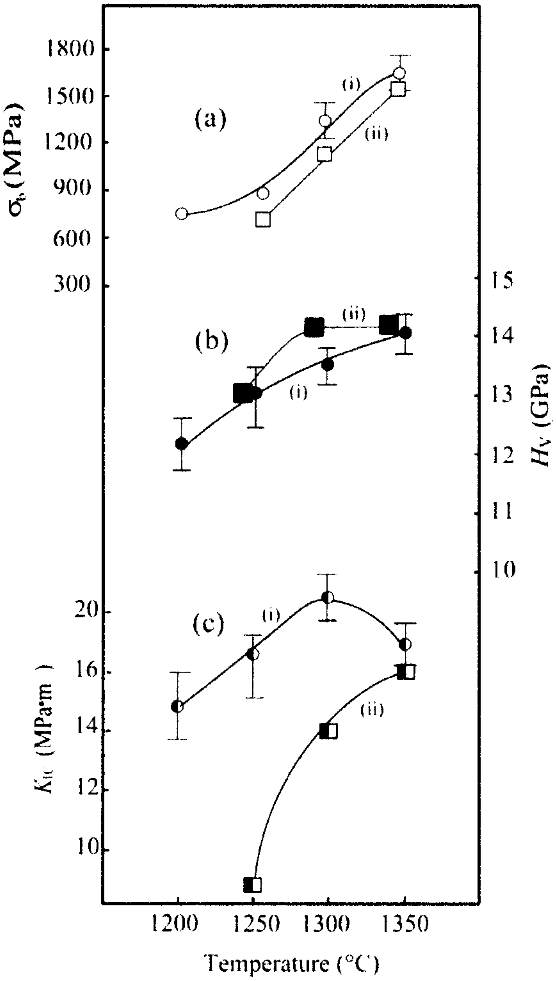

Figure 7. Mechanical properties of (a) bending strength σ_b, (b) Vickers hardness H_v, and (c) fracture toughness K_{IC} for (i) ZrO_2(1.5Y)-25 mol%Al_2O_3 and (ii) ZrO_2(1.2Y)-25mol% Al_2O_3 composites.

In addition, small white Al_2O_3 grains (Φ100 nm) were dispersed immediately external to the ZrO_2 grains, which was the results of partial precipitation from the (*ss*) particles containing Y and Al. In another portion, Al element was recognized; this means that a small amount of Al was remained within the ZrO_2 grains, forming the (*ss*) grains. These Al_2O_3 grains might have much effect on the stabilization of ZrO_2. However, Y_2O_3 grains were not recognized from EDS line analysis; they stayed within the ZrO_2 grains to stabilize *t*-ZrO_2 phase.

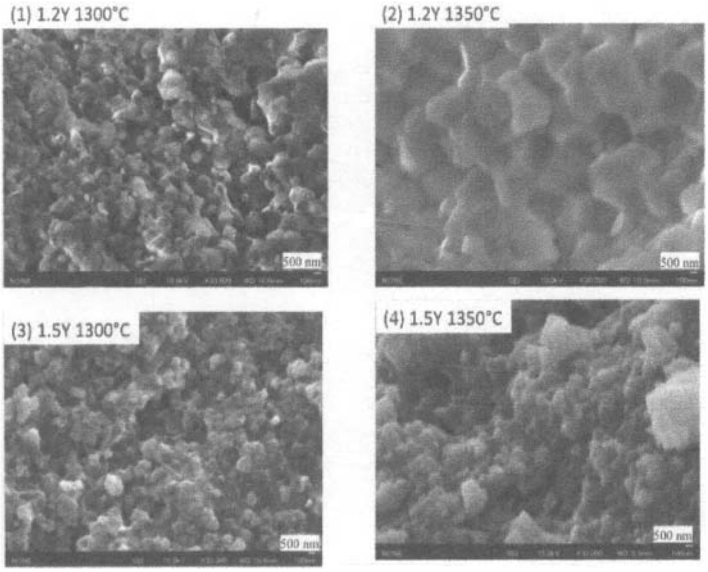

Figure 8. SEM photographs for the facture surfaces of $ZrO_2(Y_2O_3)$ -25mol% Al_2O_3 composites.

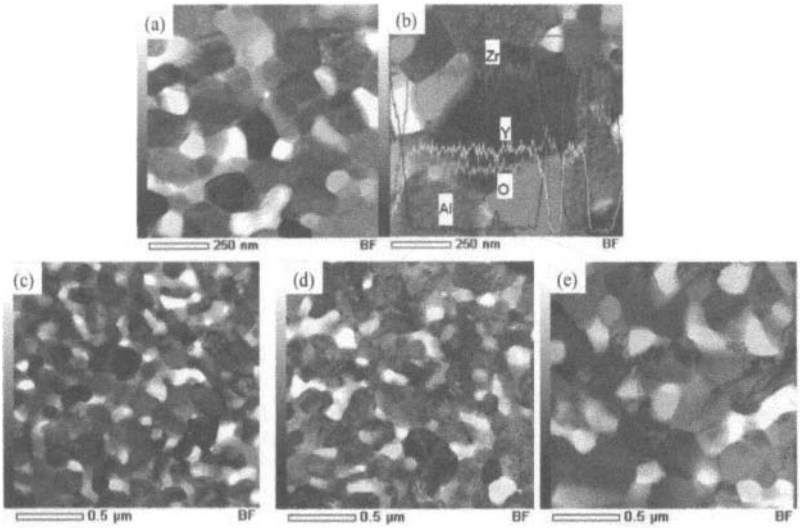

Figure 9. FE-TEM photographs for the (a) microstructural observation and (b) + line EDS analysis on $ZrO_2(1.5Y)$-25mol% Al_2O_3 ceramics sintered at 1300°C, and $ZrO_2(1.2Y)$ -25mol%Al_2O_3 sintered at 1350°C using the calcined powders at (c) 865, (d) 880, and (e) 895°C for 1 h in air.

Fig. 10 summarizes the effect of Y_2O_3 content on the mechanical properties, (a) fracture toughness K_{IC} and (b) Vickers hardness H_V, of ZrO_2-Al_2O_3 ceramics fabricated from solid solution powders; data obtained from our previous experiments are also plotted in Fig. 10, strength σ_b is omitted because the value of $\square_b$ is much affected by the relative density, and grain sizes. Off course, these curves are much different from the previous studies [18-20] in the point of the best Y_2O_3 content on the mechanical properties is a little bit small. This might be explained by the stabilizing effect from a small amount of Al_2O_3 remained in ZrO_2 grains.

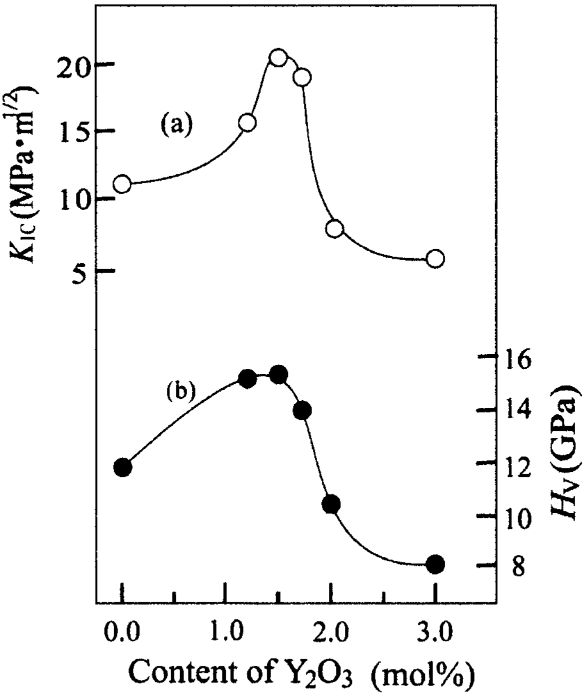

Figure 10. (a) K_{IC} and (b) H_v of ZrO_2-25mol%Al_2O_3 ceramics sintered at 1300~1350°C for 10 min under 50-60MPa in Ar as a function of Y_2O_3 content of sintered at 1300°C for 10 min under 50~60MPa.

CONCLUSIONS

By utilizing both sol-gel derived (*ss*) powders and PECPS, it has been possible to fabricate dense novel ZrO_2-based ceramics which consisted of submicron meter-size grains with a small amount of (*ss*) grain, in addition to a homogeneous distribution of α-Al_2O_3 close to fine *t*-ZrO_2 grains. These ceramics showed extreme high strength and high toughness simultaneously, which has been ever reported. These properties can introduce the ceramics into the wide industrial applications.

ACKNOWLEDGMENTS

This work was financially supported by the Ministry of Education, Culture, Sports, Science and Technology, Japan, the project S1311036.

REFERENCES

[1]R. C. Garvie, R. H. J. Hannink and R. T. Pascoe, Ceramic Steel?, *Nature* (London), **258**, (5537), 703-704 (1975).

[2]T. K. Gupta, F. F. Lange and J. H. Bechtold, Effect of stress-induced phase transformation on the properties of polycrystalline zirconia containing metastable tetragonal phase, *J. Mater. Sci.*, **13**, 1464-1470 (1978).

[3]N. Claussen, Stress Induced Transformation of Tetragonal ZrO_2 Particles in Ceramic Matrices, *J. Am. Ceram. Soc.*, **61**, 85-86 (1978).

[4]R. Ruhle, N. Clausen and A. H. Heuer, Microstructural studies of Y_2O_3-containning tetragonal ZrO_2 polycrystal (Y-TZP), in Advances in Ceramics, **12**, *American Ceramic Society*, Ohio, 352 (1984).

[5]S. Hori, M. Yoshimura and S. Somiya, Strength-toughness relations in sintered and isostatically hot-pressed ZrO_2-toughned Al_2O_3, *J. Am. Ceram. Soc.*, **69**, 169-172(1986).

[6]T. Masaki, Mechanical properties of toughened ZrO_2-Y_2O_3 ceramics, *J. Am. Ceram. Soc.*, **69**, 638-640 (1986).

[7]A. M. Alper, Inter-relationship of phase equilibria, microstructure, and properties in fusion-cast ceramics, Fig. 2, p. 339 in Science of Ceramics, **3** ,edited by *G.H. Stewart, Academic Press*, London, U.K. (1967).

[8]S. Inamura, M. Miyamoto, Y. Imaida, M. Takagwa, K. Hirota and O. Yamaguchi, High fracture toughness of ZrO_2 solid- solution ceramics with nanometre grain size in the system ZrO_2–Al_2O_3, *J. Mater. Sci. Let.*, **12**, 1368-1370 (1993).

[9]M. Tokita, Trend in Advanced SPS Spark Plasma System and Technology, *J. Soc. Powder Tech. Jpn.*, **30**, 790–804 (1993).

[10]T. Tsukuma, K. Ueda, and M. Shimada, Strength and fracture toughness of isostatically hot-pressed composites of Al_2O_3 and Y_2O_3-partially-stabilised ZrO_2, *J. Am. Ceram. Soc.*, **68**, C-4 - C-5 (1985).

[11]K. Tsukuma, K. Ueda, K. Matsushita, and M. Shimada, High-temperature strength of Y_2O_3-partially-sabilized ZrO_2/Al_2O_3 composites, *J. Am. Ceram. Soc.*, **68**, C-56 - C-58 (1985).

[12] D-Y. Lee, D-J. Kim, H-J. Hwang, Mechanical Properties of Hot Isostatic Pressed (Y, Nb)-TZP/Al_2O_3 Ceramics, *J. Korean Ceram. Soc.*, **36**, 1381-1389 (1999).

[13]R. C. Garvie and P. S. Nicholson, Phase analysis in Zirconia Systems, *J. Am. Ceram. Soc.*, **55**, 303-305 (1972).

[14]Rietveld, program 'RIETAN', http://fujioizumi.verse.jp/

[15]M. I. Mendelson, Average Grain Size in Polycrystalline Ceramics, *J. Am. Ceram. Soc.*, **52**, 443–446 (1969).

[16]K. Niihara, R. Morena and D. P. H. Hasselman, Evaluation of K_{IC} of Brittle Solids by the Indentation Method with Low Crack-to-Indent Ratios, *J. Mater. Sci. Lett.*, **1**, 13-16 (1982).

[17]A. G. Evans and E. A. Charles, Fracture toughness determination by indentation, *J. Am. Ceram. Soc.*, **59**, 371-372 (1976).

[18]F. F. Lange, Transformation toughening - Part 3 Experimental observations in the ZrO_2-Y_2O_3 system, *J. Mater. Sci.*, **17**, 240-246 (1982).

[19]F. F. Lange, Transformation toughening - Part 4 Fabrication, fracture toughness and strength of Al_2O_3- ZrO_2 composites, *J. Mater. Sci.*, **17**, 247-254 (1982).

[20]R. Shikata, Y. Urata, T. Shiono, T. Nishikawa, Strengthening of Y-PSZ-Al_2O_3 composite ceramics, *J. Jpn. Soc. Powder Powder Metall.*, **37**, 357-361 (1990).

SiC MANUFACTURE VIA REACTIVE INFILTRATION

Mario Caccia and Javier Narciso
Instituto Universitario de Materiales de Alicante. Alicante University. Alicante. Spain
marioraul@ua.es

ABSTRACT: Silicon Carbide (SiC) is one of the most important advanced ceramic, due to its unique set of electrical, optical, thermal and mechanical properties. The main barrier nowadays to wider the use of SiC is its manufacturing process, which requires very high temperatures (above 2000 °C) and pressures (> 100 MPa), is time consuming and allows a non well control of the final product quality. Out of all the procedures available, reactive infiltration has proven to be the most profitable, for it minimizes temperature (1500 °C), pressure (0.1 MPa) and processing time, while enhancing product quality control. Another advantage of this method is that it is a near net shape method. Reactive infiltration consists in infiltrating a carbon porous preform with liquid silicon. During the infiltration silicon reacts with carbon to produce SiC. In the present work, we have successfully performed reactive infiltration in different carbon performs, from highly porous foams to dense carbon fiber or bulk SiC pieces. For these infiltrations, the reaction parameters, temperature, in the range 1400-1550°C, and reaction time, in the range 1-8 hours, have been studied and optimized. The evolution of the reaction and the quality of the final products obtained were assessed via different microscopy techniques and physical properties.

1 INTRODUCTION

Silicon Carbide (SiC) is an advanced ceramic of great industrial interest for it can be used in a wide range of applications. This functionality is due to the combination of excellent thermal, mechanical, chemical, electrical and optical properties[1-7]. This material has been traditionally used for polishing and cutting applications. However, the technological advances and the capability to obtain SiC single crystals have opened a whole new specter of applications, e.g. in electronics, high wear resistance C/SiC composites or the most promising ones, metal/SiC composites to be used as heatsinks[8-10]. These novel applications require larger SiC bodies with more complex geometries which cannot be easily obtained using traditional ceramic powder sintering methods. Since SiC is a covalent solid with low diffusion capacity, sintering with total elimination of porosity is not possible. Many methods exist to densify SiC powder though. Among this methods hot isostactic pressing (HIP) is the one that produces the best quality material. This process requires very high temperatures, above 2000 °C, and high pressures, around 200 MPa, is also time consuming, and thus very expensive. An alternative method to obtain almost non porous and larger SiC pieces is reactive infiltration. This procedure consists of infiltrating a carbon porous preform with liquid silicon, so that it reacts with the carbon skeleton during the infiltration, to produce SiC, according to equation 1.

$$\mathrm{Si}_{(l)} + \mathrm{C}_{(s)} \rightarrow \mathrm{SiC}_{(s)} \qquad \Delta H^{0}_{298K} = -73\ \mathrm{kJ/mol} \qquad \text{(Eq. 1)}$$

This method allows working with less severe reaction conditions. For instance no additional pressure is required since the infiltration is spontaneous, driven by capillary forces and controlled by the reaction. Reaction temperature is around 1500 °C, much lower than for other synthesis routes. An additional benefit of this method is its near net shape capability. This technique also allows to bond SiC powder particles together. For this purpose, a green preform containing the SiC particles bonded with a suitable carbon precursor like phenolic resin or pitch must be manufactured. The green preform must be then carbonized, and infiltrated with liquid silicon to obtain the SiC, also known as reaction bonded silicon carbide (RBSC). In this work this technique has been used to bond not only silicon carbide particles of different sizes together, but also to bind carbon fibers in a ceramic matrix transforming a carbon/carbon composite into a SiC/carbon composite.

SiC formation is expansive (there is an approximately 58% volume increase when a mole of amorphous carbon reacts to form a mole of SiC[1]), so in order to avoid choking-off of the pores during infiltration, the carbon preform must have a minimum density and pore diameter, being around 38 % for amorphous carbon and 58% for graphitic carbon, with pore diameters between 1-2 μm[11-13].

In the present work, a great variety of carbon preforms commercially available, were infiltrated to obtain SiC materials. The reaction product quality was assessed with different microscopy techniques, physical and mechanical properties. The reaction parameters, temperature, and dwell time, were studied and optimized for each type of preform.

2 EXPERIMENTAL PROCEDURE

2.1 MATERIALS

In the present study, four type of carbon preforms were used. These preforms were supplied by different companies and present singular geometries and microstructures as it can be observed in figure 1. The preforms used, its main characteristics and the suppliers are listed in table 1.

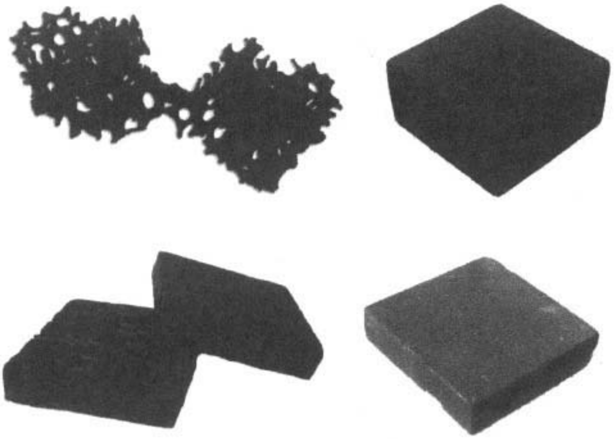

Figure 1. Different carbon preforms used for SiC composite manufacture.

Table 1. List of carbon preforms used its main characteristics.

Preform code	Composition	Supplier	Dimensions [mm]
CF	Carbon fiber, carbon binder	Brembro Brake Discs	25x25x5
SiC/C	SiC particles, carbon binder	Petroceramics	25x25x5
F	SiC particles, carbon binder	Erbicol	25x25x15
G	Partially graphitized carbon	Schunk	25x25x15

High purity Si 99.995 % supplied by Sigma Aldrich was used for infiltration tests.

2.2 INFILTRATION TESTS

Infiltrations were carried out in an horizontal tube furnace (Carbolite STF 16/75/450), in an argon atmosphere with a flow rate of 60 cm^3/min and a heating rate of 3 °C/min. Different reaction temperatures (1450-1550 °C) and dwell times (1-8 hours) were tested. Sample and silicon were put inside the furnace in an alumina boat-shaped crucible, which was previously coated with a bore nitride layer to prevent the reaction between silicon and the crucible.

2.3 MICROSTRUCTURE

Samples were cut in smaller pieces using a slow speed cutting saw Isomet from Buehler with a diamond wafer 15LC, embedded in phenolic resin and polished with proper materialographic techniques[14] summarized in table 2.

Table 2. Polishing procedure followed for microscopy evaluation of samples

Cloth	Abrasive	Lubricant	ω (rpm)	t (min)
Ultraprep	Diamond embedded 20 μm	water	200	until flatness is reached
Texmet	Diamond 15 μm paste	oil	100	30
Texmet	Diamond 6 μm paste	oil	100	30
Texmet	Diamond 1 μm paste	oil	100	30
Chemomet	Silica gel 0.1 μm	water	100	5

Microstructure was assessed with optical microscopy using reflected light in an optical microscope model PM3 from Olympus. Images were taken with a digital camera from Sony, model SSC-DC58AP using different magnifications (5x, 10x, 20x, 50x).

The porosity and pore size distribution of original preforms were characterized with mercury intrusion porosimetry using a Micrometrics Autopore IV 9500 device. Crystalline phases, both in the original preforms and in the SiC composites obtained, were identified with X ray diffraction tests, carried out in an X-Ray diffractometer Brucker model D8 advance equipped with a Cu cathode and Ni filter. Monochromatic Cu Kα radiation (λ=1.5406 Å) was used. The device operated at 40 kV and 40 mA and in the angular scanning, from 10° to 80°, a step of 0.1° and a preset time of 3 s were used. To overcome the non-planarity of the samples a Göbel mirror was used in order to work properly with a parallel optical beam. Skeletal density (ρ_s) was determined with helium picnometry using a Micrometrics Acupyc 1330TC device. Bulk density was measured using Archimedes' method using an AG204 delta range analytical balance from Mettler Toledo with a suitable kit.

3. RESULTS AND DISCUSION

3.1 GREEN PREFORM CHARACTERIZATION

The mean pore diameter (D_m), open porosity (P), skeletal (ρ_s) and bulk (ρ_b) densities of the carbon preforms are listed in table 2.

Table 3. Characteristics of the carbon preforms

Preform	P (%)	D_m (μm)	ρ_s (g/cm^3)	ρ_b (g/cm^3)
CF	24	13.4	1.8	1.16-1.25
SiC/C	30	1.3	3.1	2.15-2.19
F*	57	0.86	3.2	0.17-0.21
G	47	27.2	1.2	0.60-0.70

*Data shown is referred to the foam branches

It can be observed in table 3, that all preforms, except CF, exhibit a suitable porosity and a mean pore diameter to ensure complete infiltration without pore blocking. Even though CF preforms have a mean pore diameter wide enough to be infiltrated, the cumulative mercury plot (Figure 2) shows a wide distribution of pore sizes. Furthermore pore size distribution (Figure 3) shows that the CF preform contains pores of around 1-3 μm, which may be blocked during early stages of the infiltration. The rest of the preforms present a narrow pore size distribution around the mean value as depicted in figure 3.

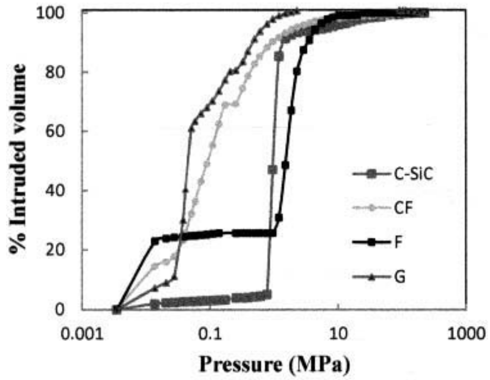

Figure 2. Mercury cumulative intruded volume vs pressure plot obtained with mercury porosimetry for all green preforms.

Taking into account that carbon fibers have a diameter of around 7 μm, when packed and oriented in one direction, they leave a star-shaped pore of around 3 μm diameter so the small pores mentioned before correspond to the holes between the fibers. The larger porosity corresponds to holes left between the fiber domains which are randomly oriented. This microstructure can be seen in figure 4, where carbon fibers are spotted as circles or ellipses depending on their orientation. Small star-shaped pores are observed between the fibers, some of them filled with the carbonized binder.